DOI: https://doi.org/10.1007/s00170-023-12623-3

The International Journal of Advanced Manufacturing Technology (2023) 129:4909–4924
https://doi.org/10.1007/s00170-023-12623-3

ORIGINAL ARTICLE

Optimising the mechanical properties of additive-manufactured recycled polylactic acid (rPLA) using single and multi-response analyses methods

Silas Z. Gebrehiwot[1,2] · Leonardo Espinosa-Leal[3] · Paula Linderbäck[2] · Heikki Remes[1]

Received: 29 June 2023 / Accepted: 27 October 2023 / Published online: 11 November 2023

Abstract
Taguchi's design of experiment (DoE) and the grey relational analysis are used to optimise fused filament fabrication (FFF) parameters for the tensile strength and modulus of toughness (MoT) responses of a recycled polylactic acid (Reform-rPLA). The paper investigates the influences of the infill geometry, infill density, infill orientation, nozzle temperature and infill speed on the mechanical properties using the L_{18} orthogonal array that is based on the $2^1 \times 4^3$ factor levels and 3 experimental repetitions. The output responses are first studied individually and combined as a multi-response optimisation using the grey relational analysis method. In the strength optimisation, the infill orientation and infill density are statistically significant with P-values α less than the 0.05 criterion. Similarly, the analysis of variance (ANOVA) for the MoT showed that infill orientation and infill geometry are statistically significant. For the multi-response optimisation, only the infill orientation is statistically significant. The mean response analyses identified factor levels that led to optimum strength and MoT responses. The confirmation tests are in good agreement with the response predictions. Using the first three influential factors, multiple variable linear regression models were developed. The predictive models showed average errors of 7.91% for the tensile strength and 8.6% for the MoT.

Keywords rPLA · Taguchi · Optimisation · Tensile Strength · Toughness

1 Introduction

Bio-based polymers are derived from renewable resources and can play a crucial role in waste reduction. The biodegradability and low carbon footprints during synthesis are the key motivations for the progress in sustainable polymer development [1]. Biodegradability is a promising trade-off for some of the properties that conventional materials such as high-performance polymers, metals and ceramics possess. There are promising developments in bio-based polymers such as polylactic acid (PLA) that can be used in the areas of biomedical engineering [2], pharmaceutical industries [3], construction [4], packaging [5] and others [1]. The Reform-rPLA is a recycled PLA developed using fully renewable sources without virgin, natural or fossil resource inclusions. Recycling PLA is regarded as a viable approach towards securing environmental sustainability [6]. Therefore, ensuring the sustainability of materials by utilising renewable sources has become a priority. However, the mechanical or thermal properties could limit their applicability in engineering. To understand the degree of trade-offs between sustainability and required material properties, thorough experimental and analytical studies are required.

Various research on mechanical behaviours of materials such as polypropylene [7], hybrid-metal composites [8–11] or natural fibre-reinforced materials [12, 13] use the fundamental approaches to reveal the short-term mechanical performances. Experimental methods are used to characterise the mechanical properties of PLA copolymers [14], metallic-reinforced PLA [15, 16], PLA and polybutylene succinate (PBS) blends [17], and PLA-pectin biocomposite [18], including nanoclays [19]. The studies focused on the

✉ Silas Z. Gebrehiwot
silas.gebrehiwot@arcada.fi

[1] Department of Mechanical Engineering, Aalto University School of Engineering, Espoo, Finland

[2] Mechanical and Sustainable Engineering, Arcada University of Applied Sciences, Helsinki, Finland

[3] Graduate School and Research, Arcada University of Applied Sciences, Helsinki, Finland

toughness and strength of the materials. The flexural rigidity of PLA beam structures with different infill densities is also experimentally studied [20], as well as the viscoelastic responses of tough-PLA with different infill densities and directions [21]. However, analytical approaches such as designing experiments (DoE) for single or multi-response optimisation objectives are required to obtain optimum performance of the materials.

The influence of various fused filament fabrication parameters on the tensile strength of PLA is studied by [22]. The single response optimisation study using the Taguchi DoE suggested that the build orientation significantly influences the strength. In addition, the mechanical properties of PLA fabricated via fused filament deposition under the influence of batch foaming [23] and gas foaming [24] methods are investigated. The Taguchi method has been successfully used to determine the optimal parameters during the fabrication of different polymer compounds, including the gasification of plastic waste [25], the influence of particle size in recycled high-density polyethylene [26] or the fabrication process via selective laser sintering (SLS) [27].

The hydrolysis rate of the PLA is studied using the L_8 orthogonal array [28]. The Taguchi DoE is also used to study the influences of infill density, printing speed, and layer thickness on the mechanical properties of PLA [29]. However, the influences on the response outputs are investigated separately, where the material's modulus and tensile strength were found optimum at 80% infill density, 40mm/s printing speed, and 0.1mm layer thickness. The influence of temperature and wall thickness on the surface roughness parameters and dimensional accuracy were studied for an additive-manufactured thin walled-PLA structure [30]. Multi-response outputs are analysed using a factorial experiment that has only two factors with three levels. The Taguchi and the response surface methods are comparatively used to optimise additive manufacturing parameters, resulting in higher compressive and tensile strengths for PLA material [31]. The signal-to-noise (SN) ratio of the response outputs is calculated. Analysis of variance (ANOVA) is used to rank the influencing factors on the quality characteristics separately, yet merely focused on comparing the approaches. Optimum printing parameters leading to good flexural and tensile properties of oil palm fibre-reinforced thermoplastic polymer are studied by [32]. The study identified the build orientation as an important parameter influencing the material's strength.

The cellular geometry, nozzle diameter and strain rate factors are studied using the Taguchi and grey relational analyse to understand their influences on toughness, stiffness and resilience [33]. The study considered factors that are less commonly correlated to the response outputs, and the factorial design suggested for the Taguchi method was not based on a standard orthogonal array. Similarly, the geometrical and mechanical properties optimisation study was carried out using grey relational analysis and the Taguchi method for 3D printed polyamide (PA6) [34]. Factors such as print temperature, print layer thickness and print speed are considered as main effects in the multi-objective analyses. Aside from the optimisation of mechanical properties, the carbon dioxide emission, printing cost and dimensional accuracy are studied using single and multi-objective DoE by [35]. Their method primarily focused on analysing the response outputs separately, and a multi-response analysis has not been carried out.

Grey relational analysis and Taguchi's methods are commonly used in multi-response optimisations of machining process parameters. This includes the optimisation of parameters for turning operation by [36, 37] and thin-film sputtering by [38]. The Taguchi method has been widely used for optimisations of key quality characteristics in machining [39–41], injection moulding [42, 43] and additive manufacturing [44, 45]. However, most of the DoE for optimisations target single response output. Multi-response outputs are studied, but only a few research focused on the optimisation of mechanical properties for the additive manufactured PLA.

The study aims to investigate the influences of 3D printing parameters on the key mechanical properties, tensile strength and MoT of a recycled PLA material manufactured by Formfutura. The reform-rPLA is a brittle material commonly used in rapid prototyping and as a component casing. The focus is on optimising the two mechanical properties; hence, a combination of a single and multi-response DoE will be used. The order of analyses in our methods follows a procedure. First, we will treat the response outputs individually as single response optimisation using the Taguchi method. A DoE using the L_{18} orthogonal array with three experimental repetitions, $n = 3$, is applied to study the relationships between the desired response outputs and factor levels. Next, we will use the combined Taguchi and grey relational analysis method for the multi-response optimisation. Finally, the influencing factor levels leading to optimum responses will be compared. Further, optimum response predictions based on the influencing factors are included.

2 Material and methods

2.1 Experimental design

The DoE in this work considers a single two-level and four three-level factors. The two-level factor is the infill geometry, an attribute based on the line and zigzag patterns. On the contrary, all the remaining three-level factors are based on variable data. The factors are infill speed, nozzle temperature, infill density and infill orientation. The entries of factor levels in the Taguchi orthogonal array are presented

using numeric symbols. The values of factor levels used are denoted by these notations. See Table 1.

In the DoE, only the main effects are considered, leading to a total of 10 degrees of freedom (DoF). The DoF is part of the statistical analysis, and for a main effect, it is one less than the number of levels of the factor [46]. Therefore, the $L_{18}\left(2^1, 3^7\right)$ orthogonal array is used. Table 2 presents the L_{18} orthogonal array with all the factors and levels assigned.

The last three columns in Table 2 are not assigned with factors; hence, they remain empty for the error analysis.

2.2 Materials and samples manufacturing

We obtained the Reform rPLA filament from Formfutura. The material is fully synthesised from renewable sources; hence, it is regarded as the most sustainable. The material is made from recycled post-industrial PLA sources and scraps from extrusions of EasyFit PLA filaments. We also used tough-PLA material for benchmarking purposes. The material is considered to have good toughness while preserving its tensile properties [47]. Our experimental method follows a procedure which starts with selecting the appropriate factorial design. Then, we use the FFF to manufacture the samples and perform the quasi-static tensile tests, see Fig. 1. Each experimental trial has three repetitions. Hence, a total of 54 experiments were carried out. The samples are designed according to the ISO 527-1B standard and manufactured using the Ultimaker S3 FFF 3D printer [48, 49]. To meet our objectives, we summarised our DoE selection, experimental procedures and result analyses in Fig. 1.

2.3 Characterisation of the mechanical properties

The static tension tests are made using the X350-20 machine from Testometric. The force and deflection data obtained from experiments are used to determine the stress–strain relations,

Table 1 Choice of factor, levels and their notations for the single and multi-response DoE using the L_{18} orthogonal array

Level notations	Factors				
	Infill geometry	Infill density (%)	Infill orientation (°)	Nozzle temperature (°C)	Infill speed (mm/s)
1	Line → 1	15 → 1	0 → 1	205 → 1	30 → 1
2	Zigzag → 2	30 → 2	45 → 2	210 → 2	40 → 2
3	-	45 → 3	90 → 3	215 → 3	50 → 3

Table 2 The Taguchi L_{18} orthogonal array used for the DoE

Experiments (test runs)	Factors							
	Infill geometry	Infill density	Infill orientation	Nozzle temperature	Infill speed	Empty column	Empty column	Empty column
						-	-	-
1	1	1	1	1	1	1	1	1
2	1	1	2	2	2	2	2	2
3	1	1	3	3	3	3	3	3
4	1	2	1	1	2	2	3	3
5	1	2	2	2	3	3	1	1
6	1	2	3	3	1	1	2	2
7	1	3	1	2	1	3	2	3
8	1	3	2	3	2	1	3	1
9	1	3	3	1	3	2	1	2
10	2	1	1	3	3	2	2	1
11	2	1	2	1	1	3	3	2
12	2	1	3	2	2	1	1	3
13	2	2	1	2	3	1	3	2
14	2	2	2	3	1	2	1	3
15	2	2	3	1	2	3	2	1
16	2	3	1	3	2	3	1	2
17	2	3	2	1	3	1	2	3
18	2	3	3	2	1	2	3	1

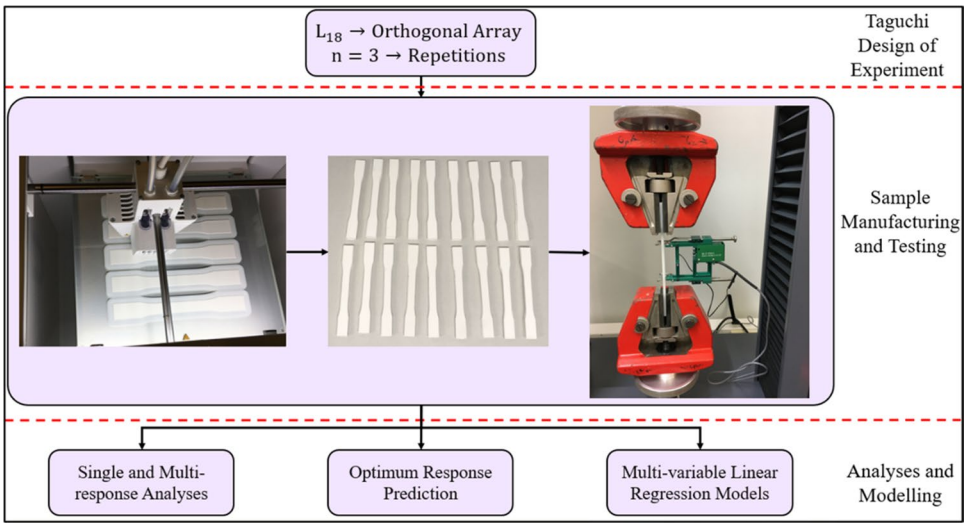

Fig. 1 The selection of DoE, experimental procedures followed and proposed analyses for optimising the response outputs

Young's modulus, tensile strength, elongation at break and toughness. The tensile strength of a material is the maximum stress reached before the material fractures. It characterises the materials' ability to support loading prior to fracture [50]. On the other hand, the elongation at break measures the ductility of a material. It characterises the material's ability to resist deformation caused by external loading. The elongation at break ε_b, is usually given as a percentage of the ratio between the change in length at break, ΔL_b and gauge length, L_o. The MoT of a material refers to the energy absorption behaviour. External loadings cause elastic or plastic deformation of the materials [50]. A tough material has a good combination of strength and ductility. In quasi-static tension, the area under the stress–strain curve up to fracture is regarded as the modulus of toughness. It measures the strain energy density of the material and is given as

$$U_t = \int_0^{\varepsilon_f} \sigma d\varepsilon. \tag{1}$$

In Eq. (1), U_t is the MoT, and ε_f is the fracture strain, the same as ε_b.

The tensile strength can be directly determined from the stress–strain data obtained via tensile testing. However, the MoT is the energy density, which can be determined by evaluating the area under the stress–strain curve, see Eq. (1). We used the trapezoidal integration rule to evaluate the MoT of the material. The stress–strain data obtained from the experiments are in the form of $\left(x_i, f\left(x_i\right)\right)$ where x_i represents the strain data, ε_i whereas $f\left(x_i\right)$ are stress data, σ_i. The stress–strain relationship of the material is based on the material's response to external deformation. Therefore, the MoT can be determined using the trapezoidal integration rule for unequal spacing, see Eq. (2).

$$\begin{aligned}\int_{\varepsilon_o}^{\varepsilon_f} \sigma d\varepsilon &= \sum_{i=1}^{n} \frac{1}{2}\left[\left(\varepsilon_i - \varepsilon_{i-1}\right)\left(\sigma\left(\varepsilon_{i-1}\right) + \sigma\left(\varepsilon_i\right)\right)\right] \\ &= \frac{1}{2}\left(\varepsilon_1 - \varepsilon_o\right)\sigma_o + \left(\varepsilon_2 - \varepsilon_o\right)\sigma_1 + \ldots \\ &\quad + \left(\varepsilon_n - \varepsilon_{n-2}\right)\sigma_{n-1} + \left(\varepsilon_n - \varepsilon_{n-1}\right)\sigma_n.\end{aligned} \tag{2}$$

In Eq. (2), n is the number of intervals considered and the initial strain $\varepsilon_o = 0$. We used a 3mm/min test speed for the mechanical testing. The experimental results of the maximum tensile strength and the MoT of the material are evaluated and presented in Table 3.

2.4 The Taguchi method

Taguchi's DoE is commonly used for analysing a single-response optimisation problem. In this paper, the optimisation aims at the tensile strength and MoT responses. The quality characteristics of both mechanical properties focus on maximising the outputs; hence, the larger-the-better SN ratio type is used to transform the responses. The larger-the-better SN ratio, η is given as [51]

$$\eta = -10\log\left[\frac{1}{n}\sum_{i=1}^{n}\frac{1}{y_i^2}\right]. \tag{3}$$

In Eq. (3), n is the number of experimental replicates, and y_i represents the response outputs considered.

Using Eq. (3), the mean response outputs are converted to SN ratios, see Table 4.

The mean responses and SN ratios are inputs to the core statistical analysis made using the ANOVA. In the

Table 3 Response outputs of the L_{18} Taguchi DoE with 3 repetitions

Test runs	Responses					
	Tensile strength (MPa)			MoT (MPa)		
	σ_1	σ_2	σ_3	U_{t1}	U_{t2}	U_{t3}
1	18.5	19.7	19.7	0.28	0.54	0.30
2	18	19.1	15.2	0.36	0.32	0.30
3	21.2	23	23.1	0.29	0.37	0.40
4	17.7	17.7	21.1	0.23	0.21	0.46
5	19.6	20.8	21.5	0.29	0.38	0.48
6	28.2	23.1	28	0.43	0.26	0.40
7	21.2	17.1	15.7	0.49	0.20	0.16
8	22.4	19.9	22.0	0.41	0.28	0.34
9	30.5	31.5	35	0.44	0.47	0.74
10	15.5	16	22	0.18	0.18	0.57
11	19.4	20.4	21	0.31	0.31	0.53
12	22.4	26.4	25.8	0.33	0.63	0.44
13	21	22.8	20.8	0.60	0.37	0.29
14	20.5	20.9	22.6	0.30	0.33	0.54
15	28.8	30.6	20.1	0.69	0.53	0.21
16	21.3	18.4	17.8	0.50	0.22	0.21
17	20.3	22.4	22.2	0.65	0.37	0.39
18	29.8	35.4	30.7	0.38	0.88	0.40

Table 4 The SN ratio for the larger-the-better quality characteristics of the response outputs

Tests	Factors					SN ratio [dB]	
	Infill pattern	Infill density	Infill orientation	Nozzle temperature	Infill speed	Tensile strength	MoT
1	1	1	1	1	1	25.70	−9.53
2	1	1	2	2	2	24.70	−9.83
3	1	1	3	3	3	27.00	−9.28
4	1	2	1	1	2	25.40	−11.85
5	1	2	2	2	3	26.27	−8.88
6	1	2	3	3	1	28.33	−9.41
7	1	3	1	2	1	24.90	−13.70
8	1	3	2	3	2	26.58	−9.51
9	1	3	3	1	3	30.14	−5.87
10	2	1	1	3	3	24.71	−13.46
11	2	1	2	1	1	26.12	−9.15
12	2	1	3	2	2	27.83	−7.57
13	2	2	1	2	3	26.65	−8.70
14	2	2	2	3	1	26.56	−8.96
15	2	2	3	1	2	28.00	−9.74
16	2	3	1	3	2	25.58	−12.12
17	2	3	2	1	3	26.68	−7.37
18	2	3	3	2	1	30.02	−6.84

statistical analysis, the F and P-values are commonly used to determine the statistical difference of the average of measurements. Commonly, a threshold of significance level P-value, $\alpha > 0.05$, invokes the null hypothesis, which

states that the means of the measurements are all equal. For $\alpha \leq 0.05$, the null hypothesis is rejected, and at least one of the means is statistically different from others [46, 51–53]. The critical F-value and the P-value are correlated using DoF of factors, DoF_1 as numerators, and DoF of error, DoF_2 as denominator [45, 50].

2.5 Multi-response using grey relation analysis

The objective of our work focuses on optimisation of the two response outputs. Hence, we combine the Taguchi method with the grey relational analysis to convert the multi-response problem into an equivalent single-response optimisation. We first normalised the response outputs for each treatment using [52]

$$x_{ij} = \frac{y_{ij} - \left(y_{ij}\right)_{\min}}{\left(y_{ij}\right)_{\max} - \left(y_{ij}\right)_{\min}}. \tag{4}$$

In Eq. (4), y_{ij} is a response output of the i^{th} test run. The $\left(y_{ij}\right)_{\min}$ and $\left(y_{ij}\right)_{\max}$ are correspondingly the minimum and maximum response outputs observed during all test runs. Then, the grey relational coefficient, GC_{ij}, of each output response is evaluated using Eq. (5) [52].

$$GC_{ij} = \frac{\Delta_{min} + \varphi\Delta_{max}}{\Delta_{ij} + \varphi\Delta_{max}}. \tag{5}$$

For the j^{th} response output, Δ_{ij} is the absolute difference between the optimum and the i^{th} normalised response values. The $\Delta_{\min}$ and $\Delta_{\max}$ are the minimum and maximum deviations of normalised responses, respectively. The distinguishing coefficient, φ, takes a value between 0 and 1. In this paper, the value of φ is adjusted to 0.5. Finally, the grey relational grade g_i of each test run is computed [53].

$$\mathrm{g}_i = \frac{1}{m}\sum_{j=1}^{m} GC_{ij}. \tag{6}$$

In Eq. (6), m refers to the number of responses considered.

2.6 Optimum response modelling

In our single- and multi-response output optimisation, we selected the levels of influencing factors to evaluate optimum responses using the predictive model β_{opt}.

$$\beta_{\mathrm{opt}} = \bar{y} + \sum_{i=1}^{k}\left(F_j - \bar{y}\right)_i. \tag{7}$$

In Eq. (7), $\bar{y}$ is the overall mean of the responses, and F_j represents the list of selected influencing k factors at different levels, i.e., $j = 1$, $j = 2$ or $j = 3$.

For a multi-factor dependent response, a linear regression can be used to predict output responses using a multiple variable regression model. The multiple variable regression model predicts the output, β as

$$\beta = \beta_o + \sum_{i=1}^{k}\beta_i F_i + \epsilon. \tag{8}$$

In Eq. (8), β_o is a constant, and β_i are regression coefficients of the influential factors, F_i. The ϵ represents experimental error.

3 Results and discussion

We used the Minitab software to evaluate the ANOVA based on the mean responses.

3.1 Single-response optimisation using Taguchi's method

The strength and MoT responses are analysed individually to determine the influential factors and levels. In addition, the response predictions are made by considering all the factors.

3.1.1 Tensile strength

The main effect plot for the mean SN ratios shows the factors and levels that lead to optimum response output, see Fig. 2.

The analysis shows that the optimum tensile strength can be achieved when the infill geometry is zigzag, the infill density is 45%, the infill orientation is at 90°, the nozzle temperature is 205°C, and the infill speed is 30mm/s. Table 5 presents the response table with a ranking order of the factors evaluated based on delta (Δ). To determine the ranking order, the mean responses are first evaluated at each factor level. Then, the Δ is calculated taking the difference between the maximum and the minimum mean responses observed at different levels. The factor with the highest Δ is the most influential, hence assigned 1st in the ranking order. The factor with the next highest Δ is assigned 2nd, and so on.

The infill orientation and density are ranked first and second, indicating that the changes made on their levels highly affect the response output. The nozzle temperature, infill speed and geometry are correspondingly ranked as third, fourth and fifth, indicating their levels' lower effects on the response output. The ANOVA of the mean responses is evaluated and presented in Table 6. The infill orientation with $\alpha = 0.00$ and infill density with $\alpha = 0.045$ are statistically significant factors.

The total percentage contribution of the sum of squares (SS) for these two factors reaches 81.3%. On the other hand, the error contributes 10.7%, representing uncontrolled noise factor from the measurement and experimental procedure, see Fig. 3.

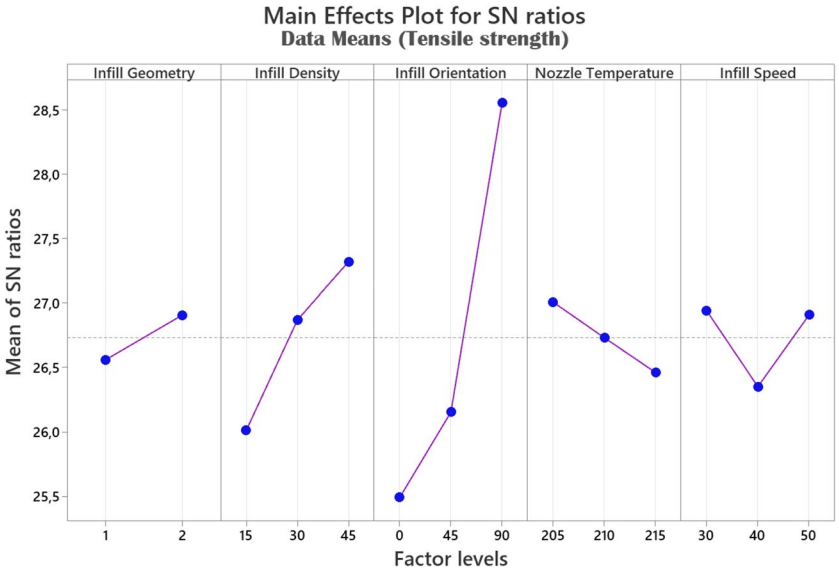

Fig. 2 The main effects of factors and levels on the mean SN ratios of tensile strength

Table 5 Mean response table for tensile strength

Levels	Factors				
	Infill geometry	Infill density	Infill orientation	Nozzle temperature	Infill speed
1	21.86	20.35	19.11	23.13	22.88
2	22.79	22.54	20.46	22.40	21.36
3	-	24.08	27.40	21.44	22.73
Delta (Δ)	0.92	3.74	9.29	1.69	1.52
Rank	5	2	1	3	4

Table 6 The ANOVA for tensile strength

Source of variation	Parameters				
	Degree of freedom (Df)	Sum of squares (SS)	Mean squares (MS)	*F*-value	*P*-value
Infill geometry	1	3.837	3.837	0.85	0.383
Infill density	2	42.295	21.147	4.69	0.045
Infill orientation	2	237.479	118.74	26.34	0.00
Nozzle temperature	2	8.613	4.307	0.96	0.425
Infill speed	2	8.388	4.194	0.93	0.433
Residual error	8	36.069	4.509		
Total	17	336.681			

3.1.2 Modulus of toughness

The main effect plot, response table and ANOVA are made to explore the influences of the factors on the quality characteristic.

Based on Fig. 4, optimum MoT can be achieved when the infill geometry is zigzag, the infill density is 45%, the infill orientation is 90°, the nozzle temperature is 205°C, and the infill speed is at 50mm/s. The ranking order in Table 7 indicates how the infill orientation and nozzle temperature highly influence the MoT.

However, the infill density which ranked second for the tensile strength, is now fourth, indicating its lower influence on MoT. On the other hand, the ANOVA shows the statistical significance of the infill orientation with $\alpha = 0.003$, infill geometry with $\alpha = 0.033$ and nozzle temperature with $\alpha = 0.038$, see Table 8.

The percentage contribution of these three factors is 74.1% of the total variation, out of which 14.2% is due to error, see Fig. 5.

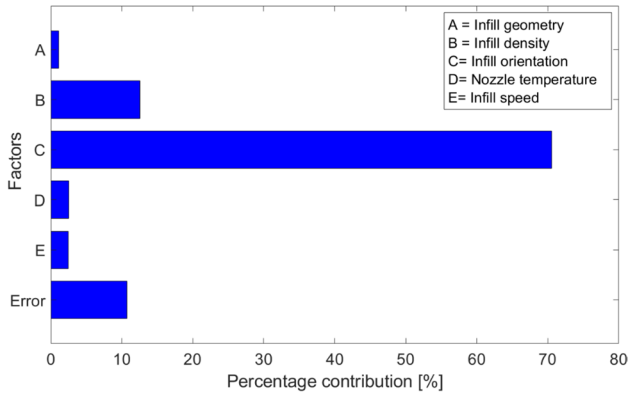

Fig. 3 Percentage contribution for variations in tensile strength due to the factors and error

3.2 Multi-response optimisation

Using Eqs. (6–8), the multi-response problem is converted into an equivalent single-response optimisation. The grey relational analysis is made, and the details of the coefficients and grades are presented in Table 9.

The single-response output formed by the grey relational grade calculation consists of fractional contributions from the multi-response outputs. The grades are used as mean responses, and the analysis on Minitab determined the statistically significant factors.

Figure 6 shows that the optimum response can be achieved by selecting zigzag infill geometry, 45% infill density, 90° infill orientation, 205°C nozzle temperature and 50mm/s infill speed parameters. The factor levels leading to an optimum multi-response output are in good agreement with the single-response optimisation analyses see Figs. 2, 4 and 6. On the other hand, Table 10 shows that the infill orientation, infill density and nozzle temperature are the influencing factors. The least influencing factor is the infill geometry.

The ANOVA of the multi-response relational grade indicated that the infill orientation with $\alpha = 0.007$ is the only statistically significant factor. Even if above the significance level, the infill density and nozzle temperature have low *P*-values and are the second and third important factors influencing the response output, see Table 11.

The infill orientation, density, and nozzle temperature make 74.32% of the SS. However, the contribution due to

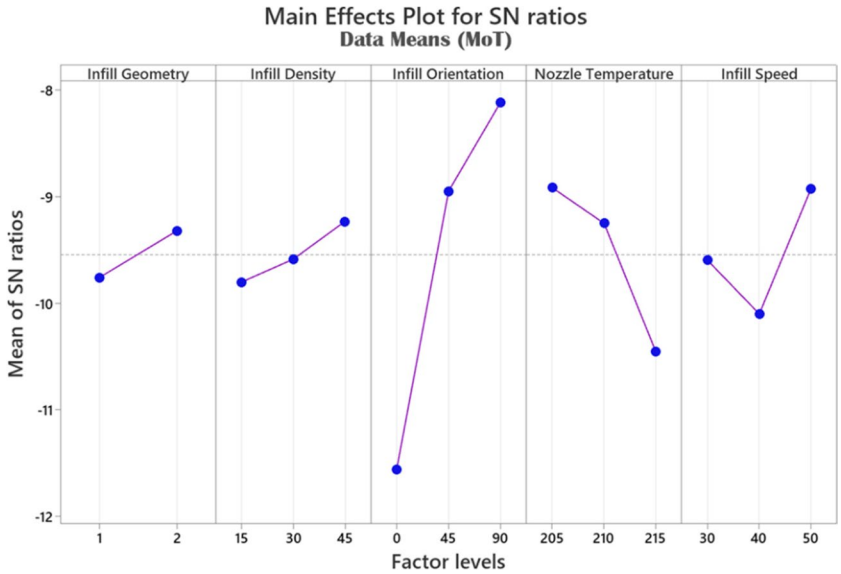

Fig. 4 The main effects of factors and levels on the mean SN ratios of MoT

Table 7 Mean response table for MoT

Levels	Factors				
	Infill geometry	Infill density	Infill orientation	Nozzle temperature	Infill speed
1	0.3644	0.3681	0.3317	0.4251	0.3916
2	0.4189	0.3890	0.3831	0.4043	0.3696
3		0.4177	0.4601	0.3455	0.4137
Delta (Δ)	0.0545	0.0496	0.1285	0.0797	0.0441
Rank	3	4	1	2	5

Table 8 The ANOVA for MoT

Source of variation	Parameters				
	Degree of freedom	Sum of squares (SS)	Mean squares (MS)	*F*-value	*P*-value
Infill geometry	1	0.013355	0.013355	6.63	0.033
Infill density	2	0.007444	0.003722	1.85	0.219
Infill orientation	2	0.050167	0.025084	12.46	0.003
Nozzle temperature	2	0.020483	0.010241	5.09	0.038
Infill speed	2	0.005824	0.002912	1.45	0.291
Residual error	8	0.016111	0.002014		
Total	17	0.113384			

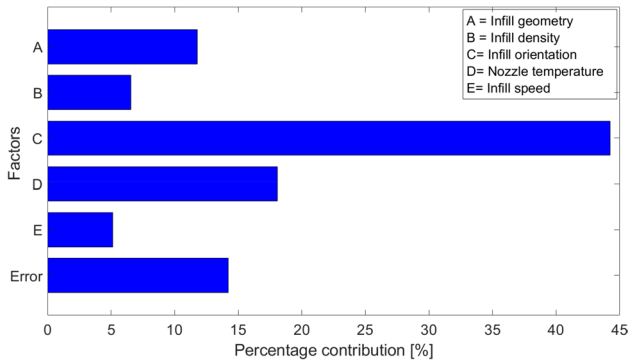

Fig. 5 Percentage contribution for variations in MoT due to the factors and error

Table 9 Grey relational analysis

Tests	Normalised scores (x_{ij})		Grey relational coefficients (GC_{ij})		
	Tensile strength	MoT	Tensile strength	MoT	Grey relational grade (g_i)
1	0.13	0.34	0.36	0.43	0.40
2	0.00	0.16	0.33	0.37	0.35
3	0.34	0.26	0.43	0.40	0.42
4	0.09	0.07	0.36	0.35	0.35
5	0.22	0.37	0.39	0.44	0.42
6	0.60	0.31	0.56	0.42	0.49
7	0.04	0.00	0.34	0.33	0.34
8	0.27	0.24	0.41	0.40	0.40
9	1.00	0.99	1.00	0.97	0.99
10	0.03	0.10	0.34	0.36	0.35
11	0.19	0.37	0.38	0.44	0.41
12	0.50	0.67	0.50	0.60	0.55
13	0.28	0.50	0.41	0.50	0.45
14	0.26	0.40	0.40	0.46	0.43
15	0.61	0.71	0.56	0.64	0.60
16	0.12	0.09	0.36	0.35	0.36
17	0.28	0.69	0.41	0.62	0.51
18	0.98	1.00	0.96	1.00	0.98

uncontrolled noise factor rises to 19.4 5%, see Fig. 7. The sources could be attributed to the analysis method, the measurement and experimental errors or the interaction of factors.

3.3 Optimum response prediction

The factor levels that lead to optimum outputs are determined for the tensile strength and MoT. The optimum responses are predicted analytically and compared to the results of the confirmation tests. The combination of factors' levels that lead to optimum responses are not included in the original L_{18} factorial design. Hence, a new set of samples is manufactured at the optimum levels. See the mean SN ratio plots in Figs. 2 and 4. Three samples are manufactured for each response and tested in tension to confirm the predictions experimentally. Table 12 presents the details of analyses on optimum response predictions.

3.4 Predictive models using influential factors

Multiple variable regression models were developed using MATLAB, considering only the first three influential factors for the strength and MoT responses. The selection of the first three influential factors is based on how small *P*-values the factors have in the ANOVA see Tables 9 and 12. Considering the main effects of all factors in the predictive models only slightly contributed to accuracy. To show that, we first developed the models using the five factors. Then, predictive models using the main effects of the first three influential factors are developed by disregarding the contributions from the least influential factors, interactions and errors. Comparing the errors of the models, the multiple variable regressions with the five factors only improved by 0.057% for the tensile strength and 0.97% for the MoT predictions. This shows that the main effects of the least influential factors do not contribute to the accuracy of the models. The cumulative deviations of the models with the three influential factors were within a maximum of 8.6% error margin. The tensile

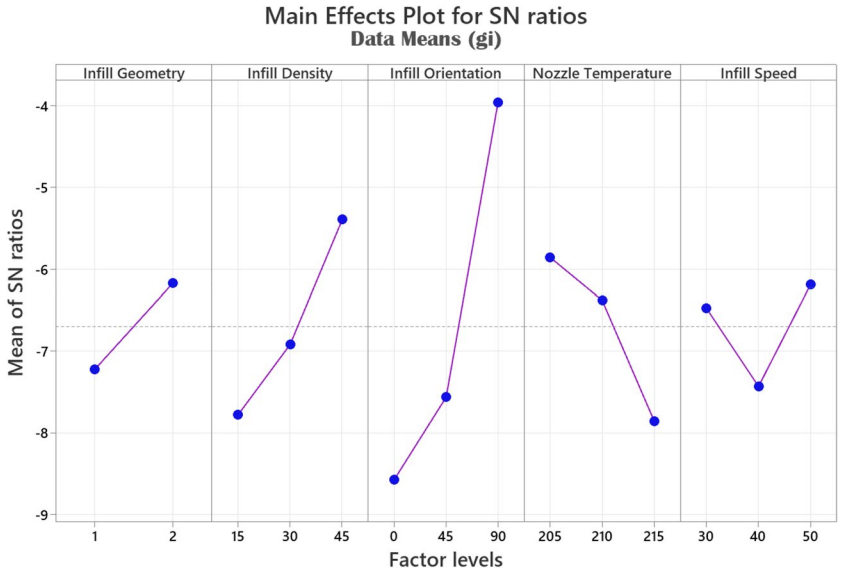

Fig. 6 Main effect of factors and levels on the mean SN ratios of grey relational grades

Table 10 Mean response table for multi-response relational grade

Levels	Factors				
	Infill geometry	Infill density	Infill orientation	Nozzle temperature	Infill speed
1	0.4610	0.4132	0.3747	0.5433	0.5075
2	0.5162	0.4568	0.4212	0.5153	0.4356
3		0.5958	0.6699	0.4073	0.5226
Delta (Δ)	0.0551	0.1827	0.2952	0.1360	0.0870
Rank	5	2	1	3	4

Table 11 The ANOVA for the multi-response relational grade

Source of variation	Parameters				
	Degree of freedom	Sum of squares (SS)	Mean squares (MS)	*F*-value	*P*-value
Infill geometry	1	0.01368	0.01368	0.88	0.375
Infill density	2	0.10921	0.05461	3.52	0.080
Infill orientation	2	0.30229	0.15115	9.76	0.007
Nozzle temperature	2	0.06189	0.03095	2.00	0.198
Infill speed	2	0.02596	0.01298	0.84	0.467
Residual error	8	0.12393	0.01549		
Total	17	0.63697			

strength and MoT of the rPLA can be modelled using the multiple variable equations presented in Table 13.

The predictive model equations are used to estimate the tensile strength and MoT responses based on the choice of factor levels in L_{18} DoE. The average error of the model for predicting the tensile strength remained at 7.91%. In comparison, the predictive model for the MoT showed an average error of 8.6%. The outcomes of the predicted responses are compared to the fractional experiments, see Fig. 8a and b.

Here, we present the images of the broken samples, see Fig. 9. Generally, the damage mechanism of the samples is a brittle fracture. However, the locations and causes of the failures are associated with the direction of the infills with respect to the loading. For the 0° infill orientation, the direction of the infill layers is perpendicular to the uniaxial tension, whereas the 45° infill orientation is at 45° to the loading direction. The samples manufactured with the 0° and 45° infill orientations fractured at the boundaries of subsequent layers. The cause of the failures is weak interfacial adhesions

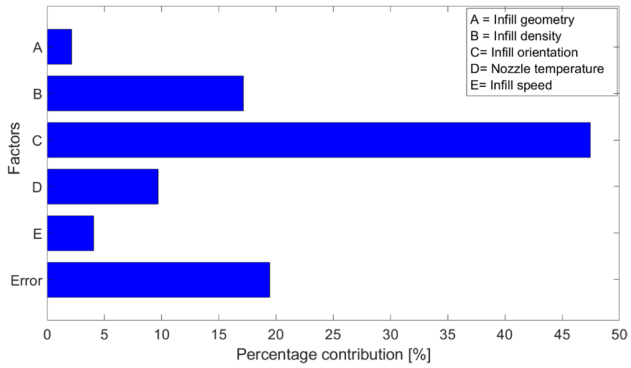

Fig. 7 Percentage contribution for variations due to factors and error in grey relational grade

between interlayers, and the locations consistently follow the infill orientations, see Fig. 9.

The 90° infill orientation samples have reinforcing infill layers towards the uniaxial loading. The fracture of the 90° infill orientation samples is due to the breakage of the infill layers, and the locations depend on the localised flaws during the infill process. These findings are also reported as tensile failure studies of 3D printed PLA [54], cracking behaviour of PLA under static loading [55], and failure characterisation of 3D printed PLA under different raster orientations [56].

Next to orientation, the infill density influenced the material's tensile strength. Our study focused on low infill density levels generally. However, the factor showed a strong correlation with the strength response. The increase in infill density increases the material's strength. This is due to the amount of material deposition increasing the infill structure of the samples. Additionally, lower infill densities create internally porous structures, which can make the samples prone to localised stress concentration during loading. In all infill orientation categories, the tensile strength of the samples monotonically increases with the infill density when a line infill geometry is used. However, for the zigzag infill, the trend of increment is observed for the 90° infill orientation. See the SN ratio presented in Table 4. The notion of increasing tensile strength with infill density is presented in several papers, including the effect of infill density on the fire properties of PLA [57], on the tensile strength [58–60], on the tensile and impact strength [61] of PLA, on the static tensile and low-cycle fatigue response of bamboo-filled PLA [62].

Next to the infill orientation, the nozzle temperature affects the MoT response of the material. The MoT is partly affected by its ductility property that depends on printing temperature [63, 64]. The nozzle temperature is a statistically significant factor for the MoT response, and the optimum response was obtained at 205°C. A stronger interlayer adhesion resulting in higher elongation at break is observed at the lower nozzle temperature. The best MoT response is exhibited by the sample in the 9th test run of the fractional experiment. The manufacturing parameters include using the 90° infill orientation and 205°C nozzle temperature for the sample variant. Nearly all of the good MoT responses of the L_{18} DoE are associated with the 205 °C, see Table 4. On the other hand, the increase in nozzle temperature generally decreased the tensile strength and MoT responses, see Figs. 2 and 4. Raising the nozzle temperature from 205°C to 215°C caused a 7.3% decrease in the strength and an 18.7% decrease in MoT mean responses. Our study shows

Table 12 Optimum response predictions and comparisons with the results of confirmation tests

Response output	Units	Optimum Levels and Factors					Response predicted	Confirmation test result	Difference
		Infill geometry	Infill density	Infill orientation	Nozzle temperature	Infill speed			
Tensile strength	MPa	2	3	3	1	1	30.98	32	1.02
MoT	MPa	2	3	3	1	3	0.53	0.608	0.0786

Table 13 Linear regression models for the strength and MoT predictions

Response output	Units	Influencing factors			Predictive model	Average errors with 3 influential factors (%)	Average errors with 5 factors (%)
		First	Second	Third			
Tensile strength	MPa	Infill orientation (o)	Infill density (d)	Nozzle temperature (t)	$49.91+(0.92\times o)+(12.45\times d)-(0.17\times t)$	7.91	7.861
MoT	MPa	Infill orientation (o)	Nozzle temperature (t)	Infill geometry (g)	$1.92+(0.0014\times o)-(0.0078\times t)+(0.054\times g)$	8.6	7.645

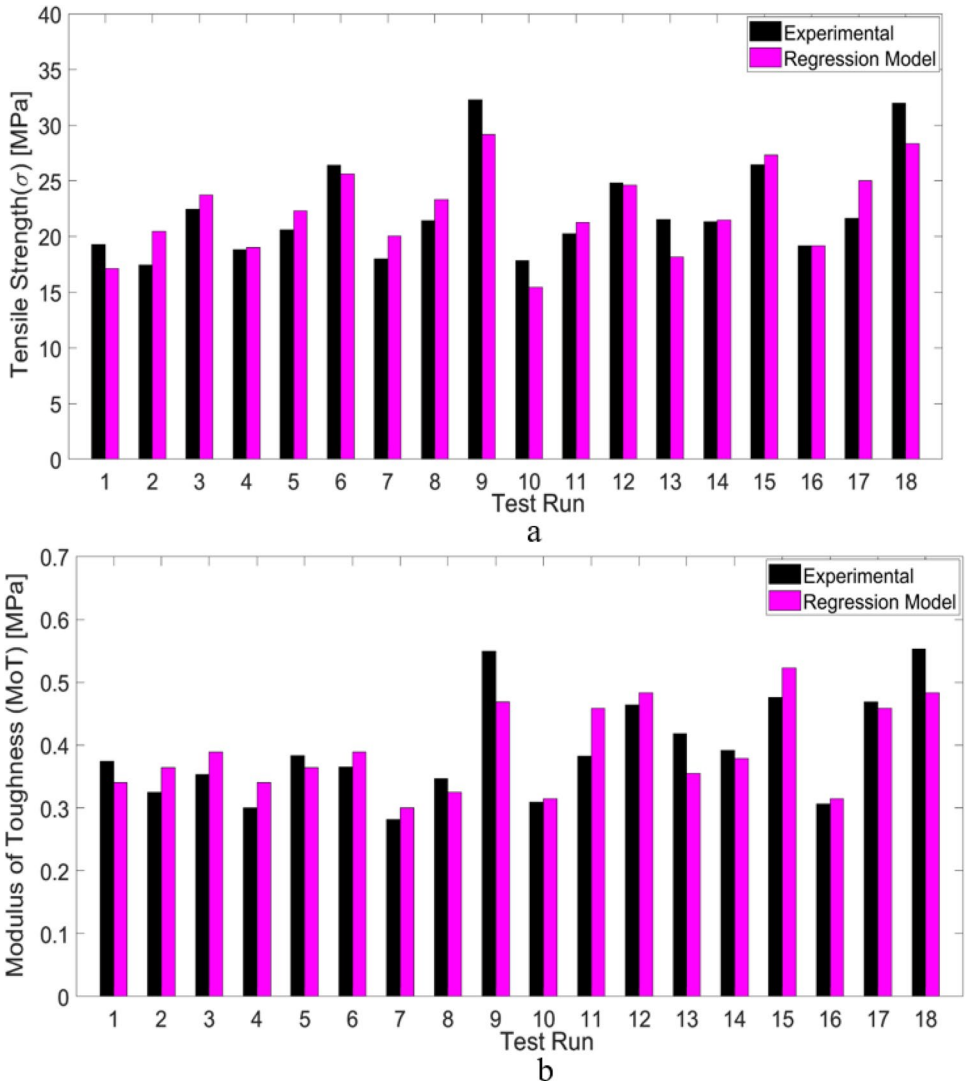

Fig. 8 Analytical predictions using the linear models compared with experimental results of (**a**) tensile strength and (**b**) MoT

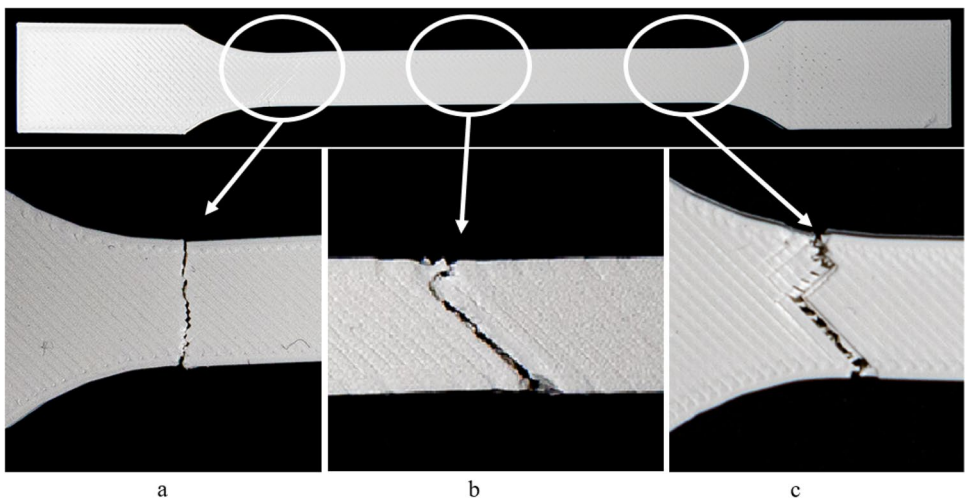

Fig. 9 Fractures of the samples selected from L_{18} DoE. **a** Test sample with 0° infill orientation and 45% infill density. **b** Test sample with 45° infill orientation and 45% infill density. **c** Test sample with 90° infill orientation, 45% infill density

no notable influences of the infill speed variations on the tensile strength and MoT of the rPLA. The studies on the mechanical properties of additive-manufactured PLA in [65] and thermoplastic composites in [66] also report the influence of nozzle temperature increment on mechanical properties. The influence of extrusion temperature on the ultimate tensile strength (UTS) of natural and coloured PLA was studied by [67]. The outcome of the study concluded that the optimum UTS for the coloured samples was obtained at 200 °C, whereas the natural PLA exhibited a maximum UTS at 230°C. The paper reports that the increments in extrusion temperature brought a decline in UTS, citing unsteady polymer melt flow as a cause during the printing processes.

The factorial experiments investigating the mechanical properties of the rPLA revealed important outcomes. Generally, the infill orientation is a key parameter that influences the mechanical properties of the studied samples. The FFF parameter variations in Taguchi's L_{18} DoE and optimum response factor levels reveal the influence of the infill orientation parameter. Although the rPLA exhibits a low-toughness behaviour and the failure is associated with brittle fracture, with the 90° infill geometry and higher infill density, its strength can be comparable and, in some cases, superior to the tough-PLA material. We present the stress–strain responses of the L_{18} DoE, as well as the rPLA and the tough-PLA manufactured using optimum parameters for strength response, see Fig. 10.

Our experimental studies showed that the material's tensile strength ranges between 17.43 and 32.29MPa, whereas the MoT ranges between 0.28 and 0.55MPa values. The variations in the responses are solely attributed to the changes in the parameters of the manufacturing processes. The analyses also indicated how the experimental designs could be used to identify combinations of factor levels that lead to optimum response predictions. The optimum response predictions are in good agreement with the results of the confirmation tests. On the other hand, theoretical response modelling using only a few influential factors can estimate the tensile strength and MoT with average errors below 10% in both cases.

4 Conclusion

The influences of 3D printing parameters on the tensile strength and MoT of the recycled PLA (reform-rPLA) are studied using the Taguchi DoE and grey relational analysis methods. The 3D printing parameters include the infill density, orientation, geometry, nozzle temperature and speed. The objective was to correlate the desired output responses with the factor levels using the single and multi-response optimisation methods. The factorial experiment was based on the L_{18} orthogonal array with $2^1 \times 3^4$ factor levels and three repetitions. The outcomes of our study are concluded as follows:

- Our single-response analyses showed that the factors and level variations influence the tensile strength and MoT. In ranking order, the infill orientation, infill density, nozzle temperature, infill speed and infill geometry affect the mean response of the tensile strength. However, the ANOVA indicated that the first two parameters are only statistically significant with the P-values $\alpha < 0.05$ criterion. On the other hand, in order of their influence on the MoT response, the infill orientation, nozzle temperature, infill geometry, infill density and infill speed are ranked 1 up to 5. According to the ANOVA, the first three factors are statistically significant. The multi-response analysis showed that the infill orientation and infill density factors are influential, but only the infill orientation is statistically significant.
- The mean response and SN ratio analyses determined the optimum settings of the factor levels for the tensile strength and MoT of the material. The optimum tensile strength can be achieved using zigzag infill geometry, 45% infill density, 90° infill orientation, 205°C nozzle temperature, and 30mm/s infill speed. The optimum MoT is obtained via zigzag infill geometry, 45% infill density, 90° infill orientation, 205°C nozzle temperature and 50mm/s infill speed parameters. The confirmation tests

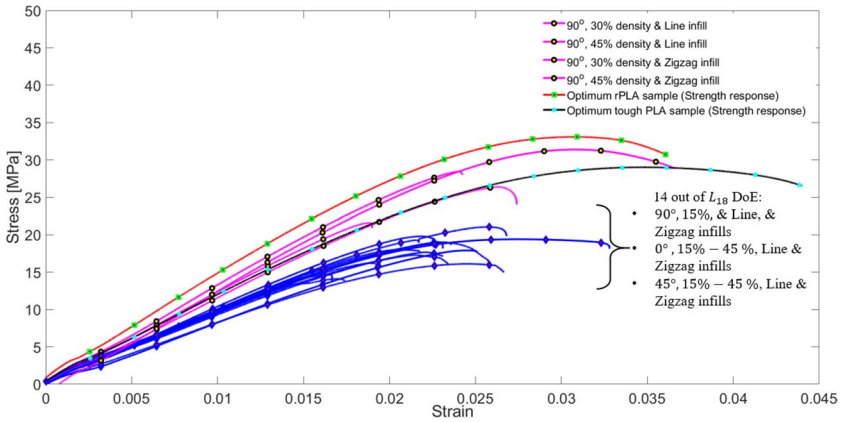

Fig. 10 Stress–strain responses of the rPLA and tough-PLA materials with different FFF parameters

proved that the errors of the optimum response predictions are notably low for both responses.

- The outcomes of the mean response analyses are used to develop multiple linear regression models for response predictions. The predictive models are fit on the experimental data using the first three influential factors. The prediction by the model for the tensile strength showed a mean deviation of 7.9%, whereas that of the MoT showed 8.6%. Considerations of all the studied factors in the predictive models did not improve the prediction errors.

The current work focused on optimisation of the mechanical property using the Taguchi and grey relational analysis and considered only the main effects. Following this, we aim to investigate interaction effects and the influences of higher infill density on the mechanical performances of the material.

Acknowledgements The authors acknowledge the Mechanical and Sustainable Engineering programme at Arcada University of Applied Sciences for providing access to materials and equipment used in this research.

Funding The first two authors, Silas Gebrehiwot and Leonardo Leonardo Espinosa-Leal received funding from TUF (Fonden för teknisk utbildning och forskning) via the project SUNSHINE (ID 332). The funds were used to cover salaries, material, and experimental costs.

Declarations

Competing interests The authors declare no competing interests.

References

1. Moshood TD, Nawanir G, Mahmud F, Mohamad F, Ahmad MH, AbdulGhani A (2022) Sustainability of biodegradable plastics: new problem or solution to solve the global plastic pollution? Curr Res Green Sustain Chem 5:100273. https://doi.org/10.1016/j.crgsc.2022.100273. (ISSN 2666-0865)
2. Ebrahimi F, Ramezani Dana H (2022) Polylactic acid (PLA) polymers: from properties to biomedical applications. Int J Polym Mater Polym Biomater 1117–1130. https://doi.org/10.1080/00914037.2021.1944140
3. Wischke H, Schwendeman SP (2008) Principles of encapsulating hydrophobic drugs in PLA/PLGA microparticles. Int J Pharm 364(2):0378–5173. https://doi.org/10.1016/j.ijpharm.2008.04.042. (ISSN 0378-5173)
4. SudamraoGetme A, Patel Brijesh (2020) A review: bio-fiber's as reinforcement in composites of polylactic acid (PLA). Mater Today: Proc 26(Part 2):2116–2122. https://doi.org/10.1016/j.matpr.2020.02.457. (ISSN 2214-7853)
5. Marano S, Laudadio E, Minnelli C, Stipa P (2022) Tailoring the barrier properties of PLA: a state-of-the-art review for food packaging applications. Polymers 14(8):1626. https://doi.org/10.3390/polym14081626
6. Zhao XG, Hwang K-J, Lee D, Kim T, Kim N (2018) Enhanced mechanical properties of self-polymerized polydopamine-coated recycled PLA filament used in 3D printing. Appl Surf Sci 441:381–387. https://doi.org/10.1016/j.apsusc.2018.01.257. (ISSN 0169-4332)
7. Gebrehiwot SZ, Espinosa-Leal L (2022) Characterising the linear viscoelastic behaviour of an injection moulding grade polypropylene polymer. Mech Time-Depend Mater 26:791–814. https://doi.org/10.1007/s11043-021-09513-0
8. Anil KC, Kumarswamy J, Reddy M, Prakash B (2022) Mechanical behaviour and fractured surface analysis of bauxite residue & graphite reinforced aluminium hybrid composites. Frattura ed IntegritàStrutturale 62:168–179. https://doi.org/10.3221/IGF-ESIS.62.12
9. Kumaraswamy J, Kumar V, Purushotham G (2021) A review on mechanical and wear properties of ASTM a 494 M gradenickel-based alloy metal matrix composites. Mater Today: Proc 37:2027–2032. https://doi.org/10.1016/j.matpr.2020.07.499
10. Jayappa K, Kumar V, Purushotham GG (2021) Effect of reinforcements on mechanical properties of nickel alloy hybrid metal matrix composites processed by sand mold technique. Appl Sci Eng Progress 14(1):44–51. https://doi.org/10.14416/j.asep.2020.11.001
11. Dhanaraj R, Venkateshwaran N, Chenthil M, Natarajan MS, Santhanam V, Baskar S (2021) Experimental investigation on the mechanical properties of glass fiber with perforated aluminum sheet reinforced epoxy composite. Mater Today: Proc 37(2021):1880–1883. https://doi.org/10.1016/j.matpr.2020.07.456
12. Santhanam V, Dhanaraj R, Chandrasekaran M, Venkateshwaran N, Baskar S (2021) Experimental investigation on the mechanical properties of woven hybrid fiber reinforced epoxy composite. Mater Today: Proc 37(2021):1850–1853. https://doi.org/10.1016/j.matpr.2020.07.444
13. Baskar S, Sendil Kumar D, Dhinakaran R, Prabhakaran A, Arun B, Shanmugam M (2021) Experimental studies on mechanical and morphological property of the natural and SBR/BR hybrid rubber. Mater Today: Proc 37:1503–1506. https://doi.org/10.1016/j.matpr.2020.07.111
14. Sin LT, Rahmat AR, Abdul Rahman WW (2013) Mechanical properties of poly (lactic acid): In Plastics Design Library. William Andrew Publishing 177–219. ISBN 9781437744590. https://doi.org/10.1016/B978-1-4377-4459-0.00005-6.
15. Zhang X, Chen L, Mulholland T et al (2019) Characterization of mechanical properties and fracture mode of PLA and copper/PLA composite part manufactured by fused deposition modeling. SN Appl Sci 1:616. https://doi.org/10.1007/s42452-019-0639-5
16. Hasanzadeh R, Mihankhah P, Azdast T, Aghaiee S, Park CB (2023) Optimization of process parameters of fused filament fabrication of polylactic acid composites reinforced by aluminum using Taguchi approach. Metals 13(6):1013
17. Qiu Z, Ikehara T, Nishi T (2003) Poly(hydroxybutyrate)/poly(butylene succinate) blends: miscibility and nonisothermal crystallization. Polymer 44(8):0032–3861. https://doi.org/10.1016/S0032-3861(03)00150-2. (ISSN 0032-3861)
18. Satsum A, Busayaporn W, Rungswang W et al (2022) Structural and mechanical properties of biodegradable poly(lactic acid) and

pectin composites: using bionucleating agent to improve crystallization behavior. Polym J 54:921–930. https://doi.org/10.1038/s41428-022-00637-9
19. Mihankhah P, Azdast T, Mohammadzadeh H, Hasanzadeh R, Aghaiee S (2023) Fused filament fabrication of biodegradable polylactic acid reinforced by nanoclay as a potential biomedical material. J Thermoplast Compos Mater 36(3):961–983
20. Gebrehiwot SZ, Espinosa Leal L, Eickhoff JN et al (2021) The influence of stiffener geometry on flexural properties of 3D printed polylactic acid (PLA) beams. Prog Addit Manuf 6:71–81. https://doi.org/10.1007/s40964-020-00146-2
21. Gebrehiwot SZ, Espinosa-Leal L, Andersson M, Remes H (2023) On the short-term creep and recovery behaviors of injection molded and additive-manufactured tough polylactic acid polymer. J Mater Eng Perform 1–19. https://doi.org/10.1007/s11665-023-08278-6
22. Hikmat M, Rostam S, Mustafa Ahmed Y (2021) Investigation of tensile property-based Taguchi method of PLA parts fabricated by FDM 3D printing technology: Results in Engineering. 11, ISSN 2590-1230.https://doi.org/10.1016/j.rineng.2021.100264
23. Azdast T, Hasanzadeh R (2021) Polylactide scaffold fabrication using a novel combination technique of fused deposition modeling and batch foaming: dimensional accuracy and structural properties. Int J Adv Manuf Technol 114:1309–1321
24. Rasouli A, Azdast T, Mohammadzadeh H, Mihankhah P, Hasanzadeh R (2022) Morphological properties and mechanical performance of polylactic acid scaffolds fabricated by a novel fused filament fabrication/gas foaming coupled method. Int J Adv Manuf Technol 119(11–12):7463–7474
25. Hasanzadeh R, Mojaver P, Chitsaz A, Mojaver M, Jalili M, Rosen MA (2022) Biomass and low-density polyethylene waste composites gasification: orthogonal array design of Taguchi technique for analysis and optimization. Int J Hydrogen Energy 47(67):28819–28832
26. Jatau S, Yawas DS, Kuburi LS, Samuel BO (2022) Production and optimization of the modulus of elasticity, modulus of rupture, and impact energy of GLP-HDPE composite materials using the robust Taguchi technique. Int J Adv Manuf Technol 121(5–6):3295–3308
27. Faraj Z, Aboussaleh M, Zaki S, Abouchadi H, Kabiri R (2022) Optimization of the parameters of the selective laser sintering for the formation of PA12 samples by the Taguchi method. Int J Adv Manuf Technol 122(3–4):1669–1677
28 Le-Shin C (2010) Optimization of biodegradability of poly (lactic acid) by Taguchi method. Polym-Plast Technol Eng. https://doi.org/10.1080/03602550903284222
29. Heidari-Rarani M, Ezati N, Sadeghi P, Badrossamay M (2020) Optimization of FDM process parameters for tensile properties of polylactic acid specimens using Taguchi design of experiment method. J Thermoplast Compos Mater. 2435–2452. https://doi.org/10.1177/0892705720964560 .
30. Aslani KE, Chaidas D, Kechagias J et al (2020) (2020) Quality performance evaluation of thin walled PLA 3D printed parts using the Taguchi method and grey relational analysis. J Manuf Mater Process 4:47. https://doi.org/10.3390/jmmp4020047
31. Gao G, Xu F, Xu J (2022) Parametric Optimization of FDM Process for improving mechanical strengths using Taguchi method and response surface method: a comparative investigation. Machines 2022(10):750. https://doi.org/10.3390/machines10090750
32. Ahmad MN, Ishak MR, Mohammad Taha M et al (2022) Application of Taguchi method to optimize the parameter of fused deposition modeling (FDM) using oil palm fiber reinforced thermoplastic composites. Polymers 2022(14):2140. https://doi.org/10.3390/polym14112140
33. John J, Devjani D, Ali S et al (2022) Optimization of 3D printed polylactic acid structures with different infill patterns using Taguchi-grey relational analysis: Advanced Industrial and Engineering Polymer Research. ISSN 2022:2542–5048. https://doi.org/10.1016/j.aiepr.2022.06.002
34. Shakeri Z, Benfriha K, Zirak N et al (2022) Mechanical strength and shape accuracy optimization of polyamide FFF parts using grey relational analysis. Sci Rep 12:13142. https://doi.org/10.1038/s41598-022-17302-z
35. Yang CJ, Wu SS (2022) Sustainable manufacturing decisions through the optimization of printing parameters in 3D printing. Appl Sci 12(19):10060. https://doi.org/10.3390/app121910060
36. Lin CL (2002) Use of the Taguchi method and grey relational analysis to optimize turning operations with multiple performance characteristics. Mater Manuf Process 19(2). https://doi.org/10.1081/AMP-120029852
37. Farhad K, Golmezerji R, Moghaddam MA et al (2012) Multi-objective optimization (MOP), simulated annealing algorithm, turning. Appl Mech Mater 110:2926–2932. https://doi.org/10.4028/www.scientific.net/AMM.110-116.2926
38. Chiang Y-M, Hsieh H-H (2009) The use of the Taguchi method with grey relational analysis to optimize the thin-film sputtering process with multiple quality characteristic in color filter manufacturing. Comput Ind Eng 56(2):648–661. https://doi.org/10.1016/j.cie.2007.12.020
39. Akıncıoğlu G, Mendi F, Çiçek A et al (2017) Taguchi optimization of machining parameters in drilling of AISI D2 steel using cryo-treated carbide drills. Sādhanā 42:213–222. https://doi.org/10.1007/s12046-017-0598-8
40. Hasçalık A, Çaydaş U (2008) Optimization of turning parameters for surface roughness and tool life based on the Taguchi method. Int J Adv Manuf Technol 38:896–903. https://doi.org/10.1007/s00170-007-1147-0
41. Julie ZZ, Joseph CC, Kirby ED (2007) Surface roughness optimization in an end-milling operation using the Taguchi design method. J Mater Process Technol 184(1–3):233–239. https://doi.org/10.1016/j.jmatprotec.2006.11.029. (ISSN 0924)
42. Chen C-P, Chuang M-T, Hsiao Y-H et al (2009) Simulation and experimental study in determining injection molding process parameters for thin-shell plastic parts via design of experiments analysis. Expert Syst Appl 36(7):0957–4174. https://doi.org/10.1016/j.eswa.2009.02.017. (ISSN 0957-4174)
43 Moayyedian M, Dinc A, Mamedov A (2021) Optimization of injection-molding process for thin-walled polypropylene part using artificial neural network and taguchi techniques. Polymers 13(23):4158. https://doi.org/10.3390/polym13234158
44. Jiang C-P, Cheng Y-C, Lin H-W et al (2022) Optimization of FDM 3D printing parameters for high strength PEEK using the Taguchi method and experimental validation. Rapid Prototyp J 28(7):1260–1271. https://doi.org/10.1108/RPJ-07-2021-0166
45. Kafshgar AR, Rostami S, Aliha MRM, Berto F (2012) Optimization of properties for 3D printed PLA material using Taguchi, ANOVA and multi-objective methodologies. Procedia Struct Integr 34(2021):71–77. https://doi.org/10.1016/j.prostr.2021.12.011. (ISSN 2452-3216)
46. Roy RK (2001) Design of experiments using the Taguchi approach: 16 steps to product and process improvement. John Wiley and Sons Inc. https://www.wiley.com/en-us/Design+of+Experiments+Using+The+Taguchi+Approach%3A+16+Steps+to+Product+and+Process+Improvement-p-9780471361015
47. ColorFabb (2022) Tough pla white. https://colorfabb.com/tough-pla-white [Accessed: November 13, 2022].
48. International Organization for Standardization (2021) Additive manufacturing — General principles — Fundamentals and vocabulary, ISO/ASTM 52900:2021. https://www.iso.org/standard/74514.html

49. International Organization for Standardization (2019) Plastics — determination of tensile properties — Part 1: General principles, ISO 527-1:2019. https://www.iso.org/standard/75824.html
50. Dowling NE (2013) Mechanical behavior of materials. Engineering methods for deformation, fracture, and fatigue, 4th edn. Pearson Education Limited, Edinburgh Gate. https://books.google.fi/books?id=OrlxMAEACAAJ
51. Yang K, El-Haik B (2003) Design for six sigma a roadmap for product development. McGraw-Hill Companies, Inc. https://www.accessengineeringlibrary.com/content/book/9780071547673
52. Krishnaiah K, Shahabudeen P (2012) Applied design of experiments and Taguchi methods. PHI Learning Private Limited. https://books.google.fi/books?id=hju9JYVhfV8C
53. Weinberg SL, Harel D, Abramowitz SK (2020) Statistics Using R An Integrative Approach. Cambridge University Press, Cambridge
54. Sabik A, Rucka M, Andrzejewska A, Wojtczak E (2022) Tensile failure study of 3D printed PLA using DIC technique and FEM analysis. Mech Mater 175(2022):104506. https://doi.org/10.1016/j.mechmat.2022.104506. (ISSN 0167-6636)
55 Ahmed AA, Susmel L (2017) Additively manufactured PLA under static loading: strength/cracking behaviour vs. deposition angle. Procedia Struct Integr 3:498–507. https://doi.org/10.1016/j.prostr.2017.04.060. (ISSN 2452-3216)
56. Khosravani MR, Berto F, Ayatollahi MR et al (2022) Characterization of 3D-printed PLA parts with different raster orientations and printing speeds. Sci Rep 12:1016. https://doi.org/10.1038/s41598-022-05005-4
57 Mensah RF, Edström DA, Lundberg O et al (2022) The effect of infill density on the fire properties of polylactic acid 3D printed parts: a short communication. Polym Test 111:107594. https://doi.org/10.1016/j.polymertesting.2022.107594. (ISSN 0142-9418)
58. Ambati SS, Ambatipudi R (2022) Effect of infill density and infill pattern on the mechanical properties of 3D printed PLA parts. Mater Today: Proc 64(Part 1):804–807. https://doi.org/10.1016/j.matpr.2022.05.312. (ISSN 2214-7853)
59. Fontana L, Minetola P, Iuliano L et al (2022) An investigation of the influence of 3d printing parameters on the tensile strength of PLA material. Mater Today: Proc 57(Part 2):657–663. https://doi.org/10.1016/j.matpr.2022.02.078. (ISSN 2214-7853)
60. de Freitas F, Pegado H (2023) Impact of nozzle temperature on dimensional and mechanical characteristics of low-density PLA. Int J Adv Manuf Technol 126:1629–1638. https://doi.org/10.1007/s00170-023-11236-0
61. Qamar TM, Haleem A, Suhaib M (2019) Effect of variable infill density on mechanical behaviour of 3-D printed PLA specimen: an experimental investigation. SN Appl Sci 1:1701. https://doi.org/10.1007/s42452-019-1744-1
62. Müller M, Jirků P, Šleger V, Mishra RK, Hromasová M, Novotný J (2022) Effect of infill density in FDM 3D printing on low-cycle stress of bamboo-filled PLA-based material. Polymers 14(22):4930. https://doi.org/10.3390/polym14224930
63. Lin CL, Lin JL (2002) Optimisation of the EDM Process based on the orthogonal array with fuzzy logic and grey relational analysis method. Int J Adv Manuf Technol 19(4). https://doi.org/10.1007/s001700200034
64. Soni K, Nayak S, Taufik AM (2021). Generation of tool path in fused filament fabrication. https://doi.org/10.1007/978-981-16-3033-0_14
65. Jagadeesh P, Puttegowda M, Girijappa YGT et al (2021). Mechanical, electrical and thermal behaviour of additively manufactured thermoplastic composites for high performance applications. https://doi.org/10.1007/978-981-16-3184-9_7
66. Olivera F, Chica E, Colorado HA (2022) Evaluation of recyclable thermoplastics for the manufacturing of wind turbines blades H-Darrieushttps://doi.org/10.1007/978-3-030-92373-0_33
67. Frunzaverde D et al (2022) The Influence of the printing temperature and the filament color on the dimensional accuracy, tensile strength, and friction performance of FFF-printed PLA specimens. Polymers 14(10):1978. https://doi.org/10.3390/polym14101978